Research in Astron. Astrophys. **2011** Vol. **11** No. **9**, 1111–1122
http://www.raa-journal.org *http://www.iop.org/journals/raa*

Research in Astronomy and Astrophysics

An experimental indoor phasing system based on active optics using dispersed Hartmann sensing technology in the visible waveband *

Yong Zhang[1,2], Gen-Rong Liu[1,2], Yue-Fei Wang[1,2], Ye-Ping Li[1,2], Ya-Jun Zhang[1,2], Liang Zhang[1,2,3], Yi-Zhong Zeng[1,2] and Jie Zhang[1,2,3]

[1] National Astronomical Observatories / Nanjing Institute of Astronomical Optics & Technology, Chinese Academy of Sciences, Nanjing 210042, China; *yzh@niaot.ac.cn*
[2] Key Laboratory of Astronomical Optics & Technology, Nanjing Institute of Astronomical Optics & Technology, Chinese Academy of Sciences, Nanjing 210042, China
[3] Graduate University of Chinese Academy of Sciences, Beijing 100049, China

Received 2011 January 31; accepted 2011 April 18

Abstract A telescope with a larger primary mirror can collect much more light and resolve objects much better than one with a smaller mirror, and so the larger version is always pursued by astronomers and astronomical technicians. Instead of using a monolithic primary mirror, more and more large telescopes, which are currently being planned or in construction, have adopted a segmented primary mirror design. Therefore, how to sense and phase such a primary mirror is a key issue for the future of extremely large optical/infrared telescopes. The Dispersed Fringe Sensor (DFS), or Dispersed Hartmann Sensor (DHS), is a non-contact method using broadband point light sources and it can estimate the piston by the two-directional spectrum formed by the transmissive grating's dispersion and lenslet array. Thus it can implement the combination of co-focusing by Shack-Hartmann technology and phasing by dispersed fringe sensing technologies such as the template-mapping method and the Hartmann method. We introduce the successful design, construction and alignment of our dispersed Hartmann sensor together with its design principles and simulations. We also conduct many successful real phasing tests and phasing corrections in the visible waveband using our existing indoor segmented mirror optics platform. Finally, some conclusions are reached based on the test and correction of experimental results.

Key words: astronomical instrumentation — methods and techniques — instrumentation: active optics — adaptive optics

1 INTRODUCTION

To collect more light and to increase resolution and sensitivity, researchers have expended tremendous efforts in recent years to increase the size of telescopic primary mirrors. Large primary mirrors

* Supported by the National Natural Science Foundation of China.

with excellent performance in their optical system can give much sharper images, since the angular resolutions of telescopes are improved. The difficulty in manufacturing a large telescope is the fabrication of the primary mirror. Monolithic primary mirrors with diameters much larger than 8 m are unfeasible owing to difficulties in support, transportation and manufacture, so segmented mirror active optics has been widely adopted in the construction of large telescopes, such as Keck, the Thirty Meter Telescope (TMT), the European Extremely Large Telescope (E-ELT) and the James Webb Space Telescope (JWST). If the segments are manufactured and positioned perfectly, the optical performance of the mirror is identical to that of a mirror with a continuous surface, except for the light missing through the small gaps between segments. This kind of phasing segmented active optics technology, especially the phase sensing technology, is regarded as one of the key technologies for extremely large telescopes.

However, for segmented mirrors, there are many challenges in the fabrication and testing process, especially the latter. A segmented primary mirror requires that all segments of the primary mirror need to be correctly phased together to ensure that the mosaic of segments has the same optical shape as an ideal single continuous surface. The phasing procedure includes phase calibration of the pistons to zero between all neighboring edges and maintaining the zero pistons with edge sensors. In this paper, we mainly focus on the former phase calibration of zero pistons with our piston sensor.

In the above mentioned large telescope projects, phasing technology is an especially important key technology and should be developed and demonstrated before the construction of an extremely large telescope. The Guoshoujing Telescope (LAMOST) project is presently the only large telescope in China, and was completed on 2009 June 4. Before the approval of the LAMOST project, Prof. Dingqiang Su successfully led the set up of two indoor active optics experimental systems in the Nanjing Institute of Astronomical Optics and Technology, Chinese Academy of Sciences (NIAOT, CAS). One is for deformable mirror active optics research and the other (Fig. 1) is for segmented mirror active optics research, which have obtained three phased hexagonal segments in the visible waveband. The success of both systems in the last century laid an important foundation for the establishment of the LAMOST project (Su et al. 1998; Wang et al. 1996; Su & Cui 2004; Su et al. 1994, 2000; Zhang et al. 2004; Zhang & Cui 2005; Zhang et al. 2002; Zhang 2006; Li et al. 2002; Cui

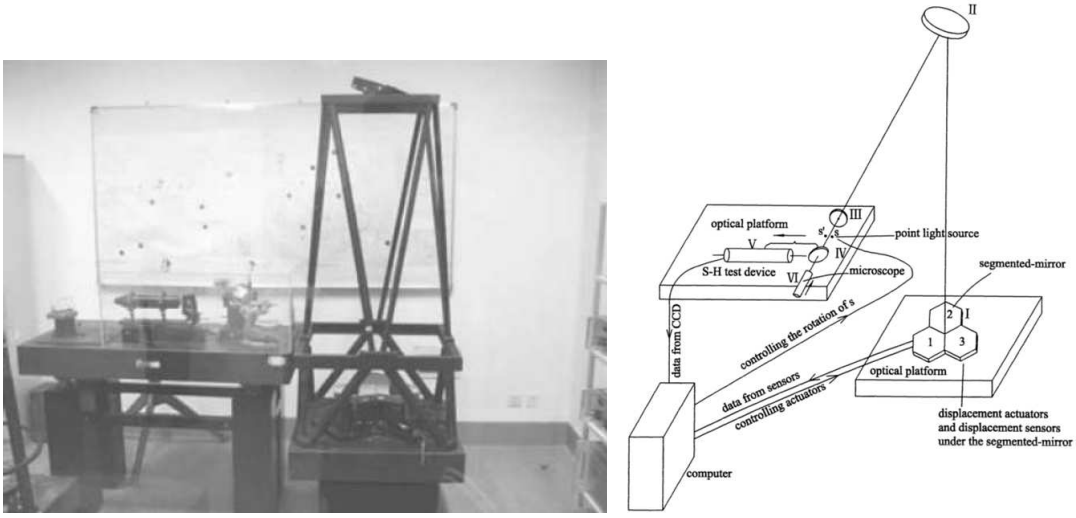

Fig. 1 Indoor segmented active optics experiment system built in 1994 at NIAOT.

et al. 2004; Yuan et al. 2006). LAMOST began with them. Now many segmented mirror telescope plans with even larger diameters are being proposed for developing Chinese astronomy.

The Dispersed Fringe Sensor (DFS) and Dispersed Hartmann Sensor (DHS) (Wirth 2000; Shi et al. 2006; Smith et al. 2003; Albanese et al. 2006) are efficient and robotic methods adopted for the JWST coarse phasing during its initial deployment. DFS for use in astronomical telescopes has been demonstrated successfully on the Keck and JWST testbeds for very coarse phasing with a piston larger than several microns. Unlike the widely used Shack-Hartmann wavefront sensor and the curvature wavefront sensor with edge sensors for calibration of relative pistons between segments, DFS can only estimate the piston by the spectrum formed with the transmissive grating's dispersion and therefore can replace the edge sensors. This type of system is difficult to calibrate.

The shortcoming of DFS is that, as the piston difference falls below one wave, its sensitivity declines markedly. This is, however, just the range in which the Hartmann Piston sensor provides high precision estimates of the piston difference. By combining the two techniques into the DHS, both a large piston range and high measurement precision are possible. The DHS could be used in two modes. When the phase step is large, the image is analyzed along the dispersion direction to yield an estimate of the phase error. This estimate is used to correct the error until the size of the step is reduced below 1/2 wave. At this point, the cross-dispersion centroid information becomes unambiguous and the error may be further reduced. Simulations indicate that the measurement of phase step errors of less than 1/50 wave should be possible. This sensor can integrate the functions of both coarse and fine phase measurement into one optical system by testing a piston in a wide measurement range from tens of microns to several nanometers.

For implementing the above new sensor and utilizing the new dispersed fringe sensing technology, we built an indoor mirror visible phasing experiment system (Zhang et al. 2009; Zhang et al. 2010a; Zhang et al. 2010c,b; Zhang & Zhang 2010) based on active optics dispersed fringe sensing technology from 2008 to 2010. Now we have tested the sensor on the original indoor segmented mirror active optics platform and already achieved results reaching the project's requirements of piston measurement accuracy of less than one-tenth of a visible 650 nm wavelength in the piston range from zero to 20 μm.

2 CONFIGURATION AND DESIGN OF THE EXPERIMENTAL SYSTEM

The system includes sensor and test platform designs and alignments of optics, mechanics, electronics and software. Figure 2 shows the optical layout.

The DHS experimental system will be tested in an auto-collimated light path and Figure 3 shows the real experimental system, including the piston sensor (on the left) and the tested segmented

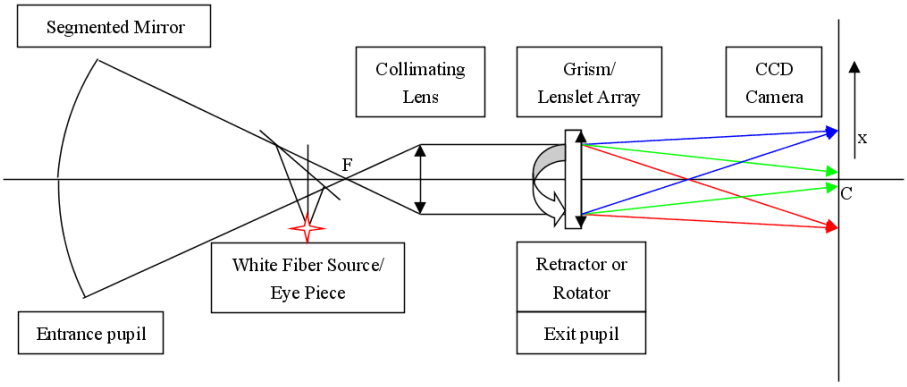

Fig. 2 System test layout of phasing segmented active optics DHS.

mirror active optics platform including three active supported segments (on the right). Among the DHS's design, there are mainly three key components: a Hartmann lenslet array, a grism and a CCD camera in the main light path in Figure 4, together with the optimized optical system's performance in Figure 5. Auxiliary light paths for the eyepiece and the Shack-Hartmann reference fiber light source are also necessary for the whole optical system in Figure 6.

According to Fraunhofer diffraction theory, the light illumination distribution is formed by incoherently adding all the monochromatic point spread functions and will satisfy Equations (1) and (2).

$$I(x,y) = I_0\left[1+\gamma\cos\left(\frac{2\pi}{\lambda(x)}\delta+\varphi(y)\right)\right], \tag{1}$$

$$\gamma \approx \exp[-(\sqrt{2}\pi C\delta/\lambda_0 d)^2]. \tag{2}$$

Here I_0 is the normalized illumination, γ is the fringe visibility and δ is the wavefront piston error between segments. By a special algorithm of least-square fit of the above modulated light distribution signal $I(x,y)$, the above mentioned parameters of fringe, especially piston δ, will be solved easily and accurately.

There are three hexagonal spherical segments supported on the platform to be segmented, shown in Figure 7. Each segment has a diagonal diameter of 250 mm, a curvature radius of 3000 mm and three displacement actuators are behind it (except for the fixed first segment).

During the alignment of the mirrors, there are two steps expressed in Figure 8, co-focusing the mirrors with tip/tilt alignment and phasing with a piston alignment and phasing alignment, which includes coarse phasing with a piston larger than 0.5 μm and fine phasing with a piston smaller than 0.5 μm.

There are three main software systems developed for displacement actuator control, three-mirror co-focusing tests and associated phasing piston tests. We have an iterative integrated control flow shown in Figure 9 for co-focusing and piston detection.

After all the design, alignment, software coding and tests were completed in July, 2010, the phasing experiment was carried out.

3 EXPERIMENTAL TEST

During the real test, we performed three gap measurements by rotating the grism by $\pm 120°$. The aperture mapping with the lenslet array is shown below in Figure 10.

By fine co-focus testing and correction of the three segments indoors, the remaining error of the actuator execution is only about 12 nm, corresponding to a centroiding precision of less than 0.1 pixel.

During piston detection after co-focus correction, we divided the area under scrutiny into two fields: one is a dispersed fringe sensing field with a piston range larger than half a wavelength (because of the low modulation and its induced large fitting error while the piston is very small) and the other is a dispersed Hartmann sensing field (where the piston range is less than half a wavelength). The processes are completely different, therefore the results will be given separately.

For the dispersed fringe sensing, we can achieve 0.1% piston detection precision, almost the same as expected and achieved by the JWST testbed and the Keck telescope when they applied DFS. The 0.1% detection error is the algorithm processing error in Table 1 between the simulated nominal piston and the piston measured from fringes with such a simulated nominal piston after applying as many error sources as possible. By using DFS, we have implemented a robotic sensing mechanism as shown in Figure 11.

For pistons distributed along different gaps in a segmented hexagonal mirror, the grism is rotated to increase the fringe visibility and to solve the problem of piston positioning more accurately. There are three piston position values between neighboring segments; theoretically, these pistons are in a

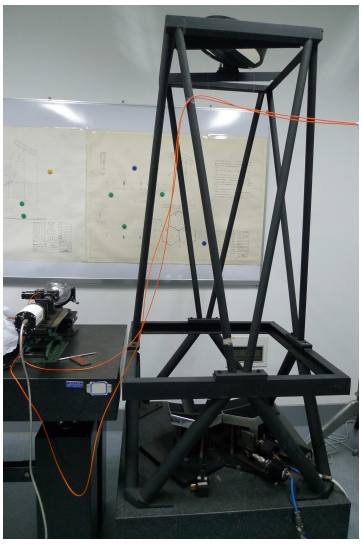

Fig. 3 Mirror phasing experiment system including sensor and platform.

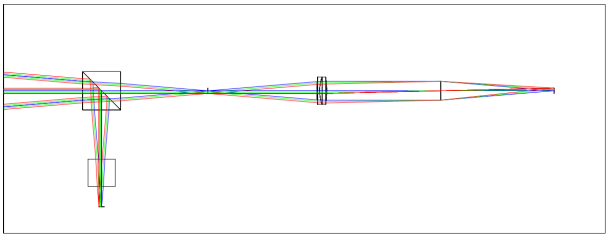

Fig. 4 DHS main light path.

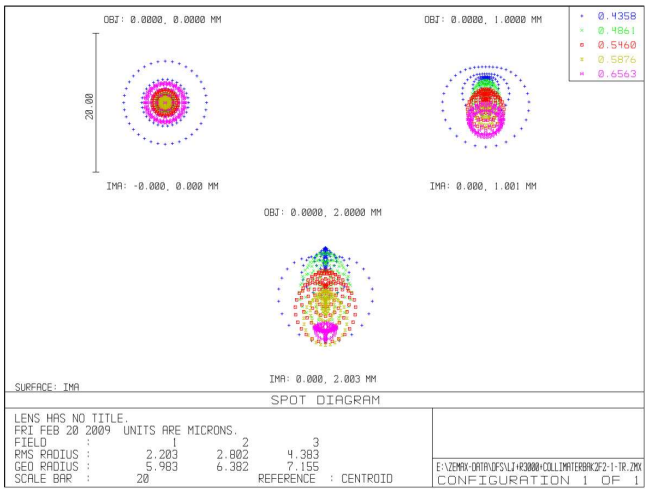

Fig. 5 DHS main light path spot diagram.

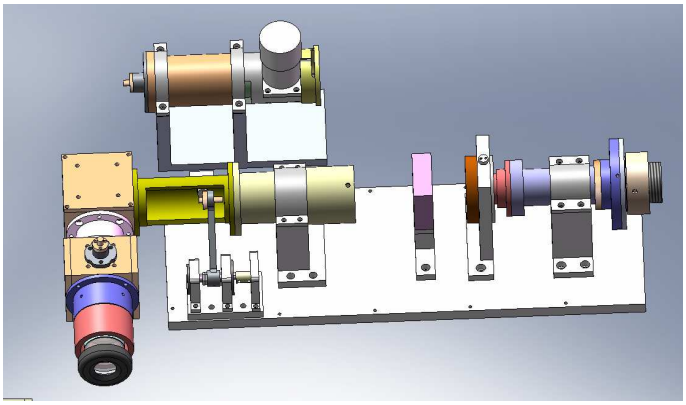

Fig. 6 DHS mechanical structure (CCD camera and some rotating mechanics are not included).

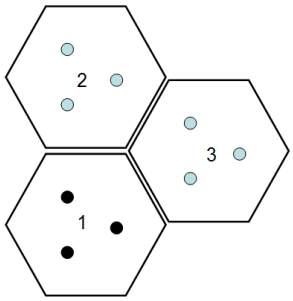

Fig. 7 Distribution of actuators on the back of the segmented mirror experiment system (Segment 1 is fixed).

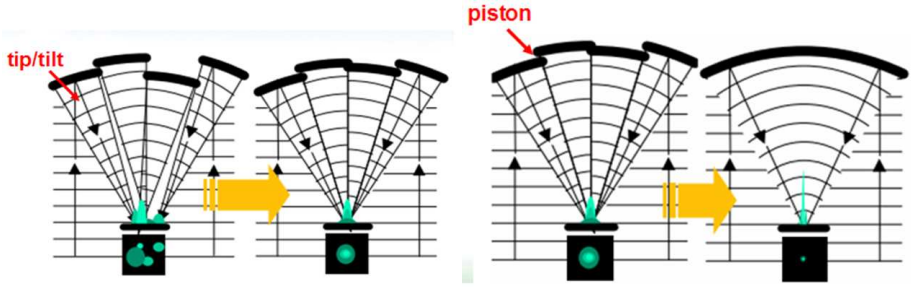

Fig. 8 Two steps of co-focusing (*left*) and phasing.

closed path and their sum is zero. We measured the three pistons below and achieved a closed path measurement accuracy of about 1 nm.

- h1=11.687μm
- h2= –9.744μm
- h3 =–1.942μm
- h1+h2+h3=0.001μm

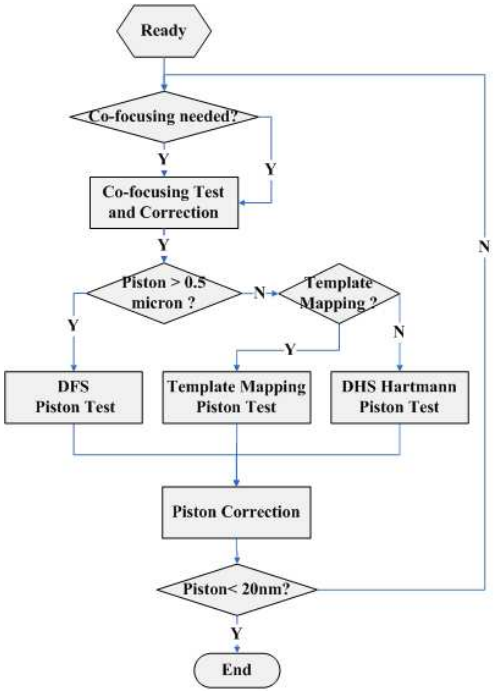

Fig. 9 Control flow.

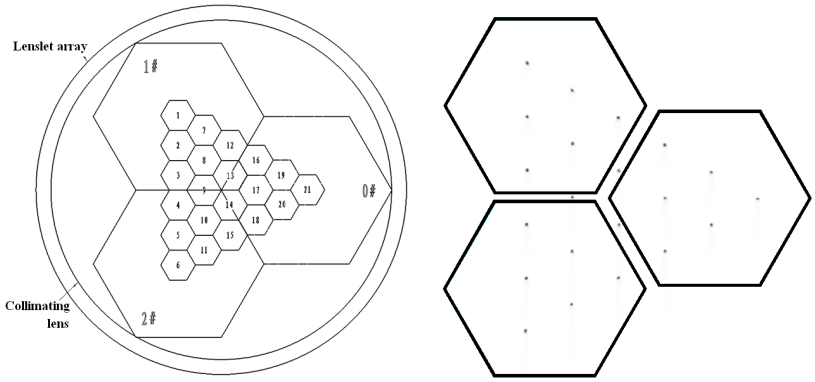

Fig. 10 Aperture mapping relation.

To detect a piston position less than about 0.5 μm, we use two methods: the dispersed Hartmann method and the template mapping method. For the dispersed Hartmann method, simulated in Figures 12 and 13, the main peak is offset from the ideal peak center where the piston's zero value is proportional to the offset.

$$dy(\lambda) = a(\lambda)\frac{\delta \cdot f}{D}. \tag{3}$$

Table 1 Dispersed Fringe Sensor (DFS) Measurement Error

Nominal Value/μm	Measurement/μm	Error/μm
0.25	0.168	–0.0815
0.35	0.386	0.0365
0.5	0.485	–0.0145
1.0	1.019	0.0195
1.5	1.495	–0.0050
2.0	1.991	–0.0090
2.5	2.496	–0.0035
5.0	5.012	0.0125
7.5	7.520	0.0205
10.0	10.024	0.0245
15.0	14.962	–0.0375
20.0	19.951	–0.0490
25.0	25.115	0.1150

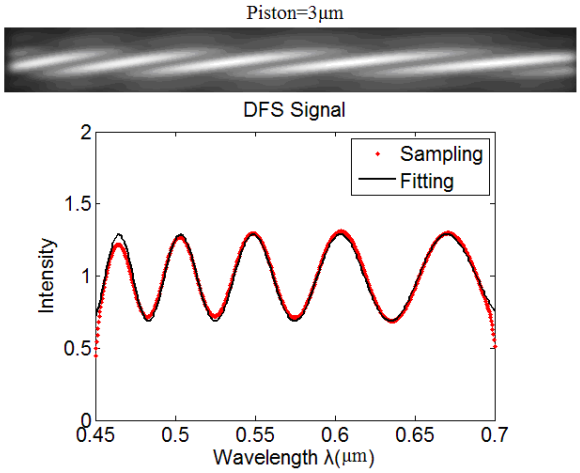

Fig. 11 Dispersed Fringe Sensor example.

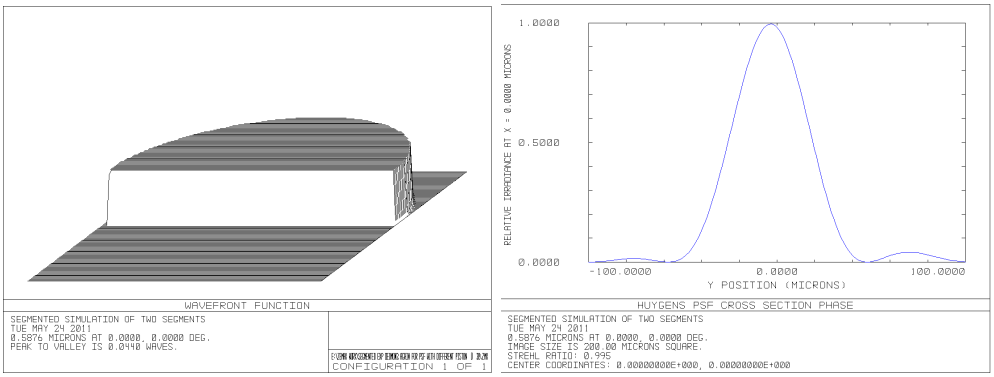

Fig. 12 Simulation and verification of the dispersed Hartmann method.

Here $a(\lambda)$ is a physical quantity expressing the diffraction effect, f is the focal length of the lenslet array, and D is the lenslet diameter. Theoretically, a centroid precision of about 0.1 pixel will correspond to a piston detection precision of 3 nm, which is the lower limit of the method.

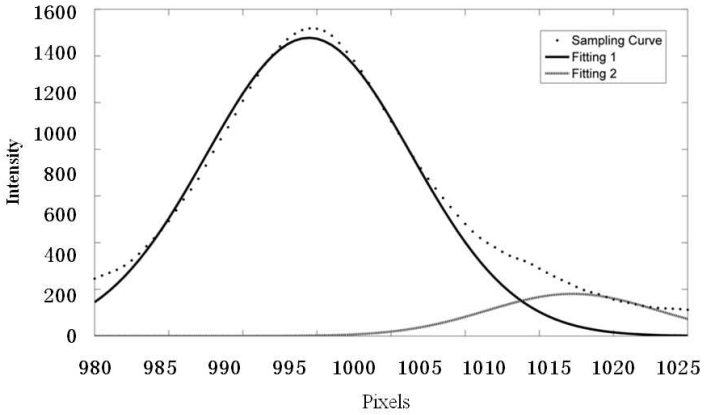

Fig. 13 Real measured piston with the dispersed Hartmann method.

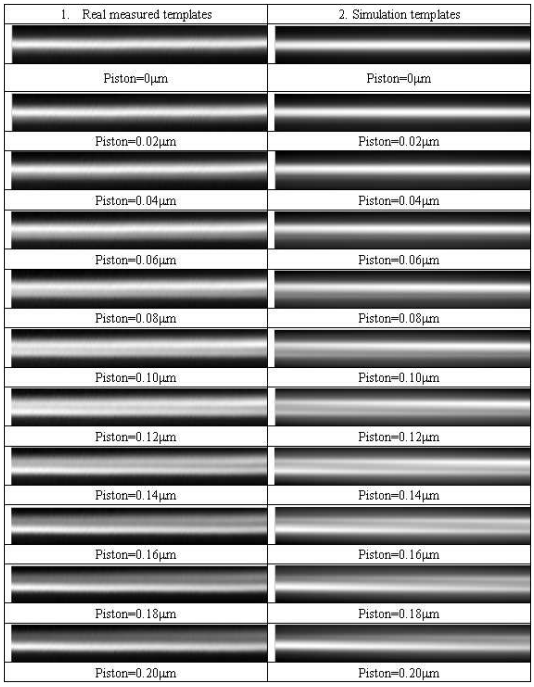

Fig. 14 Part of the simulated templates and measured templates.

The traditional template mapping method is effective and has been widely used. The Keck telescope applied this method during the narrow band phasing test. During template mapping, a series of templates, constructed either by simulation calculation or real measurements, have to be built ahead of time. During the real test, cross correlation operations between real images and templates

are carried out.

$$r = \frac{\sum_m \sum_n (A_{mn} - \overline{A})(B_{mn} - \overline{B})}{\sqrt{(\sum_m \sum_n (A_{mn} - \overline{A})^2)(\sum_m \sum_n B_{mn} - \overline{B})^2}}. \quad (4)$$

Here r is the correlation coefficient, $0 < r < 1$, and A and B are the real image fringe matrix and template matrix, respectively. Bigger r means better mapping and the biggest mapping coefficient corresponds to the most accurate piston values. We have built a template image matrix database with piston values ranging from –1 to 1 μm with a template piston interval of 20 nm in Figure 14. Because

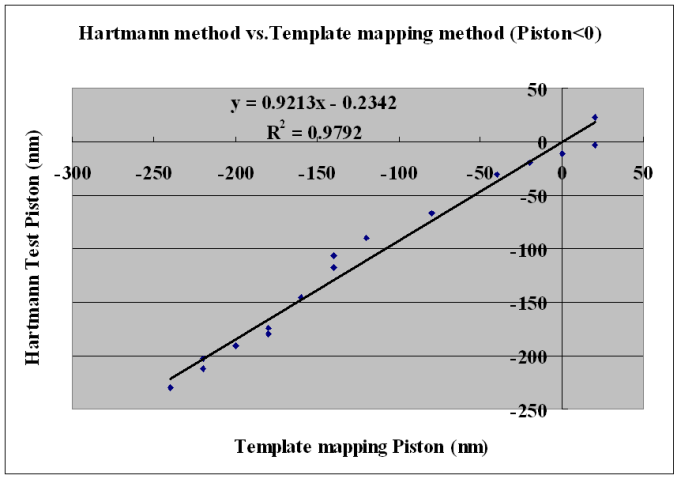

Fig. 15 Result of comparison between the Hartmann method and the template mapping method while a piston's value is less than zero and the actuators move backward.

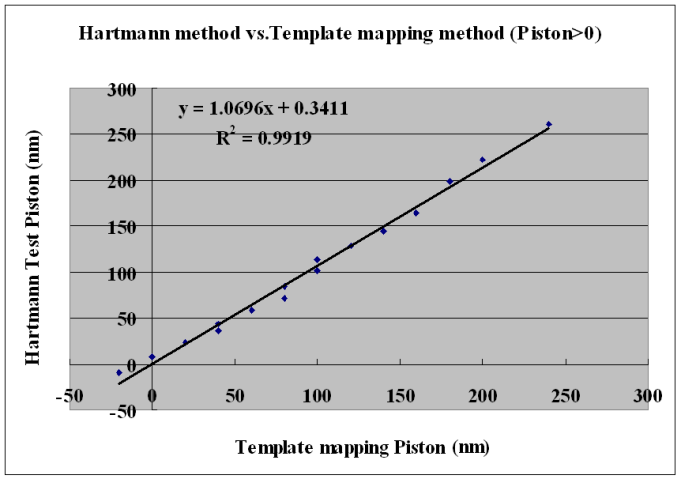

Fig. 16 Result of comparison between the Hartmann method and the template mapping method while a piston's value is larger than zero and the actuators move forward.

the human eye can descern fringe changes for a 20 nm piston change, this can help us to ensure the correct displacement actuator's behavior and respondence to control commands, despite the existing backlash. These actuators have been demonstrated to function within tolerances of 20 nm and with a theoretical resolution of 5.8 nm.

Real measured templates with piston displacements larger than 0.2 μm have been abandoned because of the displacement actuator's inconsistent performance, which introduces the misalignment of segments occurring in a large actuation.

During experiments, we have successfully measured a piston with precision of about 20 nm (including the remaining error disturbance) with both methods and implemented the mutual validation in Figures 15 and 16 after calibrating 15 nm of systemic error between the two methods, which is caused by wavelength calibration. Some correlation results between the two methods are given below.

4 CONCLUSIONS

As is well known, DFS is adopted by JWST's coarse phasing, which can lower the relative piston error to about several microns. It is a big problem to extend the minimum limit to one tenth of a wavelength because the scale is about several tens of nanometers. Based on Dispersed Fringe Sensor and Dispersed Hartmann Sensor theories, we have built a DFS/DHS type sensor including optics, mechanics, electronics and a software system, and now the sensor has already been used to successfully test pistons and phase align the lab segmented mirror experimental system in the visible waveband. After fine co-focusing with an accuracy of about 12 nm and careful wavelength calibration with two very narrow filters, the combination of the dispersed Hartmann method and the template mapping method works well within a piston accuracy of 20 nm in the visible waveband. Further work on phasing maintenance by edge sensors will be carried out with the increased support of more funds.

Acknowledgements This work was supported by the National Natural Science Foundation of China (Grant Nos. 10703008 and 11073035) and also partly supported by the Knowledge Innovation Program of the Chinese Academy of Sciences (Grant No. KJCX2-YW-T17). We sincerely acknowledge our colleagues, Liang Chen and Jinhu Lü for their great help and contributions.

References

Albanese, M., Wirth, A., Jankevics, A., et al. 2006, in Society of Photo-Optical Instrumentation Engineers (SPIE) Conference Series (Space Telescopes and Instrumentation I: Optical, Infrared and Millimeter), ed. J. C. Mather (Orlando, SPIE), 6265

Cui, X., Su, D., Li, G., et al. 2004, in Society of Photo-Optical Instrumentation Engineers (SPIE) Conference Series (Ground-based Telescopes), ed. J. M. Oschmann (Glasgow, SPIE), 974

Li, Y. P., Cui, X. Q., & Zhang, Y. 2002, in Proc. of Chinese Astronomical Telescope and Instrumentation Conference (in Chinese), ed. X. Q. Cui (Chongqing, China Science & Technology Press), 100

Shi, F., Basinger, S. A., & Redding, D. C. 2006, in Society of Photo-Optical Instrumentation Engineers (SPIE) Conference Series (Space Telescopes and Instrumentation I: Optical, Infrared and Millimeter), ed. J. C. Mather (Orlando, SPIE), 6265

Smith, E. H., Vasudevan, G., Reardon, R. D., Bernier, R., & Triebes, K. J. 2003, in Society of Photo-Optical Instrumentation Engineers (SPIE) Conference Series, ed. J. C. Mather, 4850, 469

Su, D. Q., Cui, X., Wang, Y., & Yao, Z. 1998, in Society of Photo-Optical Instrumentation Engineers (SPIE) Conference Series (Advanced Technology Optical/IR Telescopes VI), ed. L. M. Stepp, 3352, 76

Su, D.-Q., & Cui, X.-Q. 2004, ChJAA (Chin. J. Astron. Astrophys.), 4, 1

Su, D.-Q., Jiang, S.-T., Zou, W.-Y., et al. 1994, in Society of Photo-Optical Instrumentation Engineers (SPIE) Conference Series (Advanced Technology Optical Telescopes V), ed. L. M. Stepp (Kona, SPIE), 2199, 609
Su, D.-Q., Zou, W., Zhang, Z., et al. 2000, in Society of Photo-Optical Instrumentation Engineers (SPIE) Conference Series (Optical Design, Materials, Fabrications and Maintenance), ed. P. Dierickx, 4003, 417
Wang, S.-G., Su, D.-Q., Chu, Y.-Q., Cui, X., & Wang, Y.-N. 1996, Appl. Opt., 35, 5155
Wirth, A. 2000, in Society of Photo-Optical Instrumentation Engineers (SPIE) Conference Series (Optical Design, Materials, Fabrications and Maintenance), ed. P. Dierickx, 4003, 250
Yuan, X., Cui, X., Liu, G., Zhang, Y., & Qi, Y. 2006, in Society of Photo-Optical Instrumentation Engineers (SPIE) Conference Series (Advances in Adaptive Optics II), 6272
Zhang, Y., Cui, X., Liu, G., et al. 2010a, Proc. SPIE (Ground-based and Airborne Telescopes III), eds. L. M. Stepp, R. Gilmozzi, & H. J. Helen, 7733 (SPIE, Bellingham, WA 2010) 773352
Zhang, Y., Yang, D., Li, Y., et al. 2010b, Proc. SPIE (Ground-based and Airborne Telescopes III), eds. L. M. Stepp, R. Gilmozzi, & H. J. Helen, 7733 (SPIE, Bellingham, WA 2010) 77333M
Zhang, Y. 2006, in Society of Photo-Optical Instrumentation Engineers (SPIE) Conference Series (Ground-based and Airborne Telescopes), ed. L. M. Stepp (Orlando, SPIE), 6267
Zhang, Y., & Cui, X.-Q. 2005, ChJAA (Chin. J. Astron. Astrophys.), 5, 302
Zhang, Y., Li, Y. P., Yang, D. H., et al. 2002, in Proc. of Chinese Astronomical Telescope and Instrumentation Conference (in Chinese), ed. X. Q. Cui (Chongqing: China Science & Technology Press), 70
Zhang, Y., Liu, G.-R., Wang, Y.-F., et al. 2009, RAA (Research in Astronomy and Astrophysics), 9, 945
Zhang, Y., Yang, D., & Cui, X. 2004, Appl. Opt., 43, 729
Zhang, Y., Zhang, Z., & Zhang, Y. 2010c, in Society of Photo-Optical Instrumentation Engineers (SPIE) Conference Series, eds. B. L. Ellerbroek, M. Hart, N. Hubin & P. L. Wizinowich (San Diego, SPIE), 7736
Zhang, Y., & Zhang, L. 2010, Journal of Graduate School of the Chinese Academy of Sciences (in Chinese), 27, L471